Journal of Metals, Materials and Minerals, Vol. 31, No. 2, pp. 62-70, 2021

Laser powder bed fusion of Ti6Al4V-xCu: Process parameters

Thywill Ccphas DZOGBEWU[1,*]

[1] *Department of Mechanical and Mechatronics Engineering, Central University of Technology, Free State, 9301 Bloemfontein, South Africa*

***Corresponding author e-mail:** tdzogbewu@cut.ac.za

Received date:
20 January 2021
Revised date
15 April 2021
Accepted date:
23 April 2021

Keywords:
Process parameters;
LPBF;
Single tracks;
Single layers;
Cu

Abstract

The original intent of coating biomedical and surgical devices surface with antibacterial agents is to prevent infections. However, the difference in the material properties between the biomedical devices and the coating materials causes the coating material to spall from the biomedical devices. To address the situation, the current research focused on investigating the possibility of using laser powder bed fusion process a subset of additive manufacturing technology to *in situ* alloy 1 at% Cu with Ti6Al4V. *In situ* alloying 1 at% Cu with Ti6Al4V would lead to the production of medical and surgical devices with inbuilt antibacterial property. To determine the optimum process parameters that could be used to manufacture the Ti6Al4V- 1 at% Cu alloy, single tracks were produced over a wide range of laser powers and scanning speeds and analyzed. Process parameters of 170 W, 1.0 ms^{-1} and hatch distance of 80 µm were identified as the possible optimum process parameters for manufacturing the Ti6Al4V- 1 at% Cu alloy. Rescanning was identified as a good strategy to improve the surface roughness, homogeneity and surface concentration of the Cu in the Ti6Al4V- 1 at% Cu alloy matrix.

1. Introduction

Ti6Al4V is a generic alloy that had widespread application in the engineering, surgical and biomedical industries and has become a reference metallic material in ASTM F standards [1], due to its unique mechanical and biocompatible properties [2]. The preference for Ti6Al4V alloy for biomedical applications above other biometals is due to the formation of thin adherent protective titanium stable oxide film in an oxidizing environment spontaneously to prevent corrosion and promote biocompatibility of the metal. It has been identified that the same surface properties that make Ti6Al4V alloy biocompatible are responsible for its surface suitability for bacterial infections [3,4]. The formation of the thin titanium oxide layer under physiological conditions is a good substrate for the adhesion of proteins and cells which can equally provoke bacterial colonization and biofilm formation on Ti6Al4V implanted medical devices surfaces; hence Ti6Al4V alloy alone cannot meet all the clinical requirements, especially the prevention of infections without the appropriate antibacterial surface coating [5].

Unfortunately, due to the great thermophysical and mechanical differences between the coating material and the metal surface, a good mechanical bonding is not achieved between the bulk Ti6Al4V alloy and the coating material, as a result, the antibacterial coating on the surface of the Ti6Al4V alloy could fall off and the medial device is exposed to infections. To overcome this limitation, antibacterial metals such as copper was incorporated into Ti6Al4V based alloy. The review of the literature reveals that the Ti6Al4V-xCu alloy manufactured by the conventional methods (casting, forging, extrusion, etc.) prevents infection of implanted medical devices and kill bacterial on contaminated surgical instruments [6-10].

With the rapid advancement in technological development and inventions, the focus of the current research is to investigate the possibility of an alternative method of producing the Ti6Al4V-xCu alloy by direct metal laser sintering (DMLS) which is also known as selective laser melting (SLM). The DMLS/SLM is a subset of additive manufacturing (AM) which belongs to the family of laser powder bed fusion (LPBF). The DMLS technology is currently considered as a renaissance of the manufacturing industry due it monolithic manufacturing strategy as opposed to the subtractive and assembling of multiply components process used by the conventional methods (Turning, milling, grinding, drilling, etc.) of manufacturing. The elimination of the assembling process would inevitably reduce the cost and time spent on manufacturing [11]. The additive manufacturing ability of the DMLS process would lead to waste reduction and manufacturing of biomedical devices and surgical instruments with complex intricate geometries (e.g. back tapers, intricate cooling channels, customized porous structures and special lattices or hollow structures) cum antibacterial properties. The technology has the advantage of producing objects with a tailored geometry based on functional requirements which would certainly improve the quality of life of implants patients [12-14].

The possibility of using this emerging technology to incorporate Cu as an antibacterial property into Ti-based alloys would greatly revolutionize the manufacturing of implanted medical devices and other surgical instruments. The DMLS technology could be used to *in situ* alloy metallic powders such as Ti6Al4V and Cu and could produce homogenous metal matrix based on the difference between the thermophysical properties of the selected elemental powders [12-14]. The successful in-situ alloying of Cu with Ti6Al4V would not only permit the manufacturing of implanted medical devices with

in-built antibacterial properties which cannot fall off but also provide the opportunity of manufacturing implanted medical devices with complex geometries. Kinnear *et al.* [15] have investigated the possibility of using DMLS manufacturing technology to produce Ti6Al4V-Cu samples. However, the authors focus mainly on the production of the single layers and 3D objects and the homogeneity of the Cu in the Ti6Al4V precursor powder. A thorough investigation of the single tracks which is the basic unit building blocks for the DMLS manufacturing process was not vigorously investigated. A vivid description of the laser-matter interaction for single tracks production is required before considering single layers and 3D objects. For the current investigation 1 at% Cu would be in situ alloyed with Ti6Al4V (ELI) (Extra Low Interstitials) because the review of the literature has proven that 1 at% Cu is enough to produce Ti6Al4V-1 at% Cu alloy with antibacterial properties [8,9,15]. Though Cu is an essential trace element which is required for human health in the formation of red blood cells, absorption and utilization of iron, metabolism of cholesterol and glucose, synthesis and release of life-sustaining proteins and enzymes [10], it is also a heavy metal and can become toxic in the human body when used in excess (>10 wt% Cu) [8-10], hence for implanted biomedical devices it must be used moderately, as a result, the current investigation would in situ alloy only 1 at% Cu with Ti6Al4V (ELI). The use of the small amount of Cu (1 at% Cu) is analogous to the steel manufacturing technology where 0.5 wt% C is enough to enormously increases the mechanical property of the steel alloy [16].

2. Materials and methods

The experiment was conducted with spherical argon atomized powders of Ti6Al4V (ELI) and Cu procured from TLS Technik GmbH. 1.36 g of Cu (thus 1 at% Cu or 1.38 wt% Cu) was mechanically mixed with 98.64 g of Ti6Al4V (ELI) until a homogenous mixture was obtained. The chemical composition of the Ti6Al4V (ELI) argon-atomized powder presented in Table 1. The chemical composition of copper powder was 99.9% Cu. The 10th, 50th and 90th percentiles of equivalent diameter (weighted by volume) of the Ti6Al4V (ELI) powder were respectively 12.6 μm, 22.9 μm, 37 μm and 9.45 μm, 21.9 μm, 37.5 μm for Cu the powder.

An EOS M280 Direct Metal Laser Sintering (DMLS) machine supplied by EOS GmbH was used for the experiment. The laser spot diameter of the machine is ~80 μm. A Ti6Al4V substrate was used with a uniform powder deposition thickness of 30 μm. Single tracks were produced at laser powers of 150 W, 170 W, and 200 W over a wide range of scanning speeds (V = 0.2 ms^{-1} to 1.7 ms^{-1}). The window of process parameters selected for the investigation was based on the standard process parameters found in the EOS data sheet [17]. It was reported that dense DMLS Ti6Al4V (ELI) samples could be produced at a laser power of 170 W at a scanning speed of 1.3 ms^{-1}. With only 1 at% Cu, it is envisaged that the optimum process parameters for manufacturing the Ti6Al4V- 1 at% Cu alloy could be obtained within the sleeted wide range of laser powers and scanning speeds.

Table 1. Elemental composition of the Ti6Al4V.

Element	Al	V	O	N	H	Fe	C	Y
Content (wt%)	6.340	3.940	0.058	0.006	0.001	0.025	0.006	0.001

All tracks were of length 0.02 m. For each scanning speed, three single tracks were produced. The samples were mounted and metallurgically prepared and etched with Kroll's reagent for optical microscopic analysis according to well-known procedures described in the literature [18]. The distribution of Cu in the Ti6Al4V (ELI) alloy matrix was determined in a scanning electron microscope (SEM) with an X-ray energy dispersive spectrometer (EDS). The surface roughness of the samples was measured with a Surftest SJ-210 portable surface roughness tester procured from Mitutoyo America Corporation.

3. Results and discussions

For the LPBF manufacturing technology, the optimum process parameters that could be used to in situ alloy elemental powder mixtures must first be determined, since the quality and mechanical properties of the final LPBF products depends on the selected process parameters. According to the review publication of Spears and Gold [19], there are about fifty (50) different LPBF processing parameters that determined the mechanical properties of the manufactured LPBF parts. However, it is generally accepted in the research community that four main process parameters influence the quality of LPBF manufactured parts, which are: laser power, scanning speed, scan spacing (hatch distance) and powder layer thickness. These four principal variables generally determine the energy inputs during the manufacturing process hence the mechanical properties of LPBF manufacture parts [20]. It is also noted that for each type of metallic powder only a particular combination of the four parameters that could yield optimum result. It is, therefore, obligatory to determine the optimum processing parameters that could be used to produce the Ti6Al4V-1 at% Cu alloy.

3.1 Single tracks

Single tracks are the basic unit building blocks for the LPBF process of manufacturing. It is the side-by-side and the layer-by-layer arrangement of the single tracks that result in a 3D object. The quality of the individual set of single tracks determined the morphology and mechanical properties of the final object. During the LPBF manufacturing process, two types of single tracks (continuous and discontinuous tracks) could be produced (Figure 1). Continuous tracks exhibit a constant track width (Figure 1(a)), while the morphology of the discontinuous tracks could be tracks that are irregularly in shape (Figure 1(b)) or droplets of solidified molten metal known as a balling effect (balls formation) [13,21].

Discontinuity of the tracks occurs when the aspect ratio of the cylindrical liquid is high (thus the ratio of the length (L) to the diameter (W) of the cylindrical liquid) [13,22,23]. Molten metal with a high aspect ratio would break down to lower their surface energy which is known as Plateau-Rayleigh instability [23]. It is also pointed out that the discontinuity of the tracks could be due to local powder arraignment, wetting, gravity, and capillary forces [11,24].

For the current experiment, only tracks produce at a laser power of 170 W from 1.0 ms^{-1} to 1.3 ms^{-1} scanning speeds were continuous. All the other combinations of the process parameters produced discontinuous tracks of irregular shapes (Figure 2) and there was no balling effect.

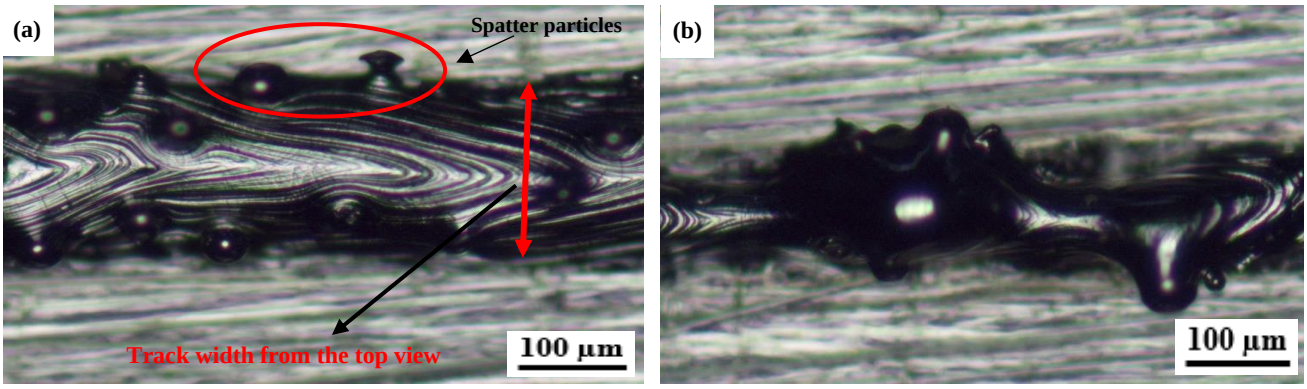

Figure 1. Morphology of the Ti6Al4V-1 at% Cu tracks: (a) continuous track, and (b) irregular track.

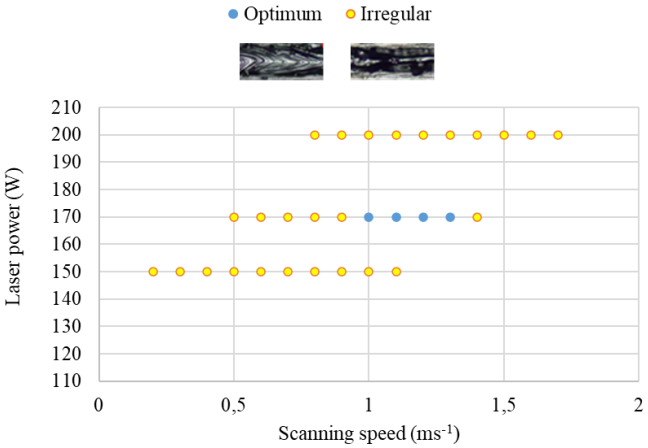

Figure 2. Morphology of the Ti6Al4V-1 at% Cu single tracks from the top view.

Spatter particles (Figure 1(a)) which were termed as satellites [22] were observed along the edge of the single tracks. Satellites are surface defects and could be formed due to "melt spattering and partial powder melting in the peripheral zone of laser spot" [25]. Since the satellites are formed at the edge of the tracks at the peripheral zone of the laser spot towards the end of the solidification process, less laser energy is transfer to them and they remain partially melted and stick to the surface of the tracks which can adversely affect the mechanical properties of the bulk material [22].

The tracks characteristics (width, height and penetration depth) of the Ti6Al4V-1 at% Cu samples were investigated (Figure 3). Measurements of the widths of the tracks from the top surface (Figure 1(a)), indicated that the widths of the tracks decrease with increasing scanning speeds (Figures 3(a-c)). During the LPBF melting process, the laser beam is absorbed initially into a thin layer of the individual powder at the surface [12]. The powder particles at the surface begin to melt and the heat proceeds into the core of the powder until a steady temperature is reached within the molten pool [13]. The hydrodynamic movement of the cylindrical molten pool depends on the linear energy input which is governed by the principal process parameters [20]. At low scanning speeds the laser energy input increase (Figure 3(d)) causing the temperature of the molting pool to increase. The high temperature in the molten pool would reduce the viscosity of the molten liquid leading to the easy flowing of a liquid phase. The large liquid phase with the low viscosity leads to the increase of the widths of the tracks with decreasing scanning speeds (Figures 3(a-c)). Conversely, a high scanning speed would lead to a reduction in the laser energy input (Figure 3(d)), causing a reduction in the temperature of the molten pool. The lower melting temperature would produce a limited molten fluid of high viscosity which would obstruct the free movement of the molten liquid hence reduction in the width of the single tracks with increasing scanning speeds. These observations of reduction in the widths of the tracks with increasing scanning speeds and the increase in the widths of the single tracks with decreasing scanning speeds aligned with what was reported in the literature [12,18].

The cross-sections of the single tracks (Figure 4) were examined to determine the extent to which the laser beam melts the powder and penetrates the substrate (the previous layer). Due to the layer-by-layer manufacturing technique of the LPBF process, the degree of 'welding' between the individual layers to form a strong metallurgical bond must be determined. The penetration depths (welding) measured for the single tracks demonstrated a great discrepancy (Figure 5).

Due to the complex mechanisms of the laser-matter interaction with a system of powder - substrate, the flows in the molten pool, the possible variable thickness of the powder layer and different particle sizes on the powder bed, lead to different track's morphology [20]. There are three types of track's profile (Figure 5) could be observed during the LPBF manufacturing process [12,13]. The first type of profile occurs when the laser energy input is not enough to melt the powder particles completely and penetrate the substrate to form a metallurgical bond, which is termed as poor penetration (Figure 5(a)). The second type of laser radiation occurs when the combination of the process parameters is able to melt the powder completely, form uniform tracks and penetrate the substrate to the desired depth to form a strong metallurgical bond with the substrate (the previous layer) (Figure 5(b)). This desired melting condition is termed the conduction mode and the combination of the process parameters that produced the desired penetration depth is referred to as the optimum process parameters [20]. The third melting condition is termed the keyhole mode of conduction and it occurs when the combination of the selected process parameters leads to high laser energy absorption into the substrate and subsequent 'drilling' of the substrate (Figure 5(c)) [22,26].

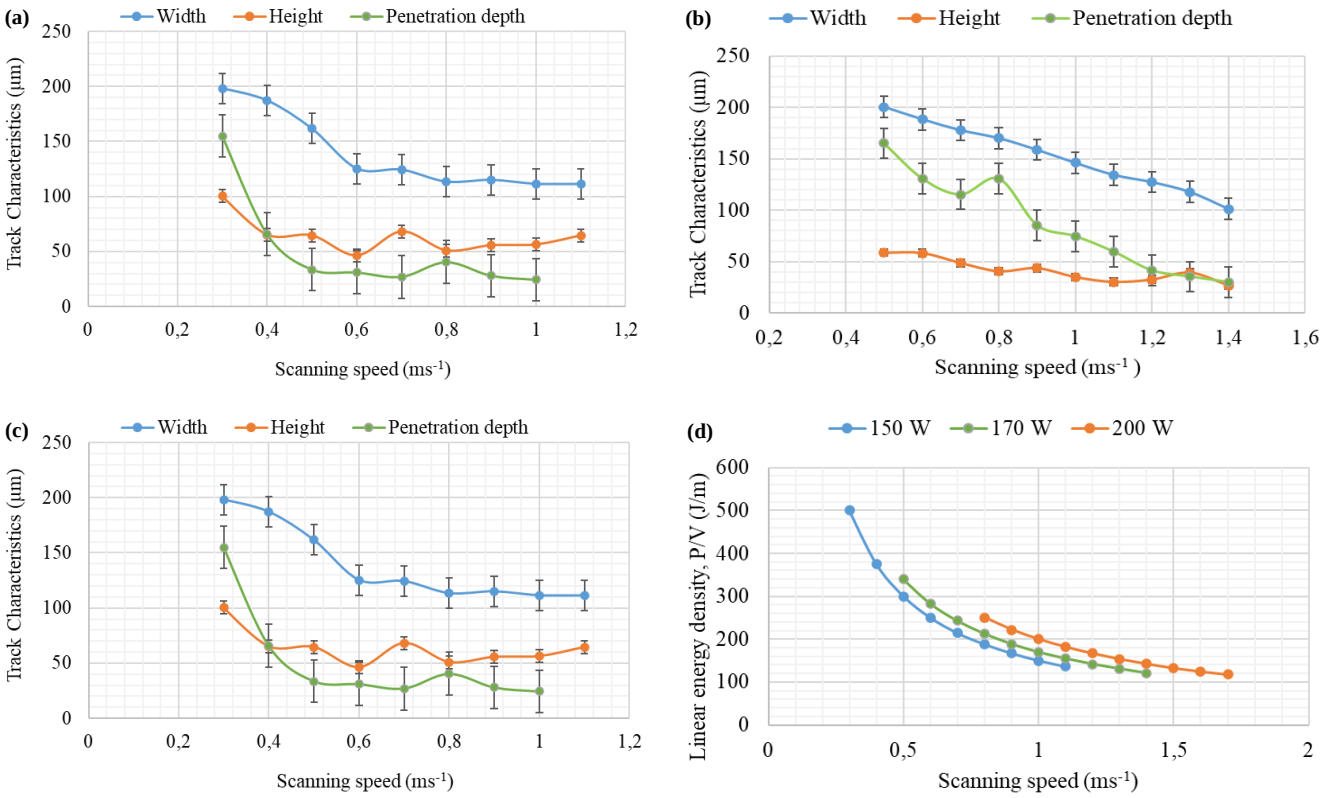

Figure 3. Tracks characteristics of the Ti6Al4V-1 at% Cu as a function of scanning speeds. (a) 150 W; (b) 170 W; (c) 200 W and (d) linear energy density (energy input).

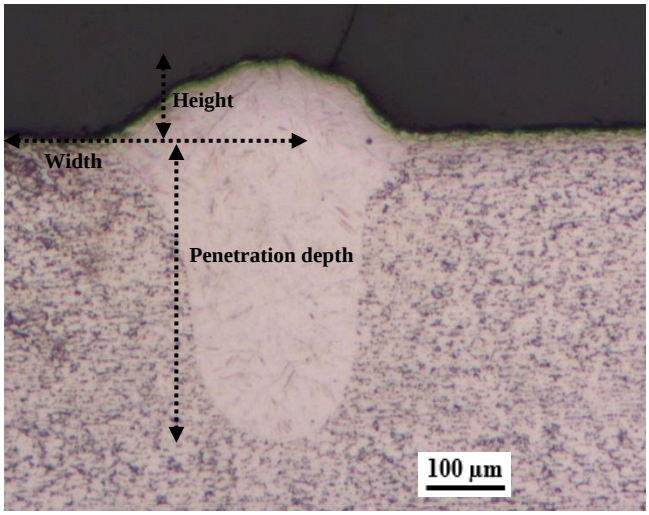

Figure 4. Measurement of the single track's characteristics from the cross-section of the Ti6Al4V-1 at% Cu alloy single tracks.

King *et al.* [27] and Eagar and Tsai [28] pointed out that at the conduction mode (optimum process parameters) the shape of the penetration depth is semi-circular 'U' shape (Figure 5(b)) whiles the keyhole mode is 'V' shape (Figure 5(c)). Yang *et al.* [29] also explained that at the conduction mode the shape of the penetration depth is greater than half the size of the width of the track. Several experimental and theoretical models have been proposed to predict the combination of the process parameters that determined the occurrence of the various types of track's profiles [29,30].

For the current experiment, only tracks produced at a laser power of 170 W with a corresponding scanning speed of 1.0 ms^{-1} resembled a 'U' shape (Figure 5(b)). The track characteristics of all the other process parameters did not meet the description of a conduction mode – 'U' shape. Single tracks produced at laser power of 150 W, 170 W and 200 W with corresponding scanning speeds from 0.2 ms^{-1} to 0.6 ms^{-1}, 0.5 ms^{-1} to 0.9 ms^{-1} and 0.8 ms^{-1} to 1.2 ms^{-1}, respectively demonstrated a keyhole mode profile (Figure 5(c)). Keyhole mode normally occurs at a low scanning speed. At a low scanning speed, the laser beam stays at a particular spot relatively for a longer time, resulting in continuous absorption of the laser radiation at that particular spot. The relatively longer radiation causes the melting of the powder particles and the subsequent 'drilling' into the substrate forming a 'V' shape (Figure 5(c)). In the keyhole mode, the laser energy density is sufficient enough to cause evaporation of the metal leading to plasma (vapour) formation. The collapse of the vapour cavity could leave a void (pore) in the wake of the laser beam which would contribute to pore defect of the final product [21,26-28]. Conversely, single tracks produce at high scanning speeds demonstrated poor penetration (Figure 5(a)). Thus - single tracks produced at laser powers of 150 W, 170 W, and 200 W with corresponding scanning speeds of 0.7 ms^{-1} to 1.1 ms^{-1}, 1.1 ms^{-1} to 1.4 ms^{-1}, and 1.3 ms^{-1} to 1.7 ms^{-1}, respectively. Tracks produced at these scanning speeds could not form a strong metallurgical bond (poor penetration) with the substrate (Figure 5(a)). At high scanning speeds, the dwelling time of the laser at a particular spot on the powder bed reduces. The short radiation time does not produce enough energy to melt the powder and form a metallurgical bond with the substrate (the previous layer) before the solidification of the molten pool.

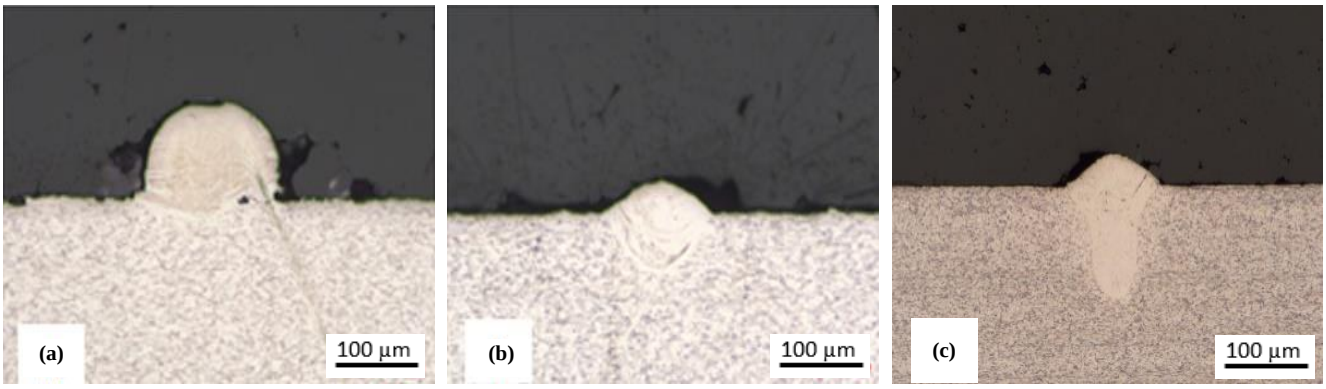

Figure 5. Cross-sectional view of the Ti6Al4V-1 at% Cu alloy single tracks. (a) Poor penetration (b) Conduction mode (c) Keyhole mode.

As depicted in Figures 3(a-c), the penetration depths of the single tracks generally decreased with increasing scanning speeds, due to the reduction in the dwelling time of the laser beam. This observation concurs with the reports of previous authors [18,31]. It is very important to note that, low or high scanning speed is always relative to the laser power. As demonstrated in the current experiment, at a laser power of 200 W with a corresponding scanning speed of 0.8 ms^{-1} produced enough laser energy to melt the powder particles completely and penetrate the substrate while laser power of 150 W with a corresponding scanning speed of 0.8 ms^{-1} could not produce enough energy to melt the powder completely and form a metallurgical bond with the substrate. This observation aligned with the statement of Yadroiesev *et al.* [24], they mentioned that process parameter are not linearly related, rather only a careful combination of the laser power and scanning speed that could yield optimum results, hence it is obligatory to determine experimentally the optimum process parameters that could be used to manufacture each type of powder blend (alloy).

The heights of the tracks also demonstrated a great inconsistency (Figure 5), especially for tracks, produce at the laser powers of 150 W and 200 W (Figures 3(a-c)). This irregularity is due to the nature of the Gaussian laser beam that melts the powder particles [32,33]. The inherent non-uniform nature of the Gaussian beam produces a non-uniform temperature gradient in the molten pool that triggers surface tension between the center and the edge of the molten pool. This temperature gradient causes recirculation flow within the molten pool leading to the oscillation of the pool surface as the molten metal solidifies forming irregular track heights [34]. During the LPBF process, the laser beam does not melt the powder particles only under the laser spot, powder particles in the immediate surrounding areas on the powder bed are also melted (denudation effect) [12,21,22], causing variation in the powder layer thickness. The variation in powder layer thickness could trigger inconsistency melt flow causing irregular track heights. The variation in powder layer thickness due to denudation effect could also contribute to the variation in penetration depth since the laser beam would melt areas with thin layers quickly and penetrate the substrate.

The measurement of the widths of the tracks from the cross-section (Figure 4) demonstrated a similar pattern as observed from the top view measurement (Figure 1(a)). Generally, the tracks widths decrease with increasing scanning speed at all the laser powers, just as observed for the top surface analysis of the track's widths (Figures 3(a-c)).

3.2 Single layers

For the LPBF manufacturing process, the single tracks are laid side-by-side to form a sing layer, hence it is important to determine the appropriate hatch distance (distance between two neighbouring single tracks) at which the single tracks could be laid side-by-side to produce the desired layer. It is the superposition of the layers that would lead to the production of a dense 3D object. While laser power and scanning speed have a major influence on single track geometry, hatch distance directly affects surface quality. For the current investigations, single layers were produced with the optimum process parameters determined from the single track's analysis – thus laser power of 170 W with the corresponding scanning speed of 1.0 ms^{-1} which have demonstrated a 'U' shape profile. Two scanning strategies (single scan and re-scan) were employed to produce the single layers at three different hatch distances (80 µm, 90 µm, and 100 µm).

From the top surface analysis, it was observed that the layers overlap completely for all the three hatch distances (Table 2). The overlapping of the layers would enable the possibility of manufacturing dense 3D Ti6Al4V-1 at% Cu samples. Satellites were visible on the surface of the single scan samples at all the hatch distances (Table 2). There is no major variation in the number of the satellites on the surfaces of the single scan samples at the different hatch distances.

The presence of the satellites would negatively impact on the surface quality of the layers. The surface quality of a DMLS sample needs to meet the industrial requirements especially sectors like the medical industry where precisely tailored surface quality is required for each type of implanted medical device. This is because implanted medical devices' surface would be in direct contact with the human body tissue for osseointegration to occur. It is empirically proven that the anchoring process after implantation is directly affected by the surface quality of the implanted devices. Due to the influence of surface quality on the loading protocol (healing process), the morphology of the LPBF manufactured surface is of prime importance [35-37].

Table 2. Ti6Al4V-1 at% Cu single layers top surface at different hatch distance.

	Single scan		
	80 µm	**90 µm**	**100 µm**
Top view of single layers	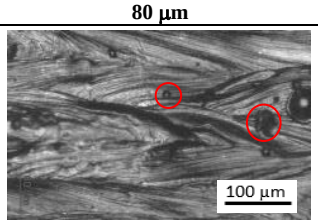	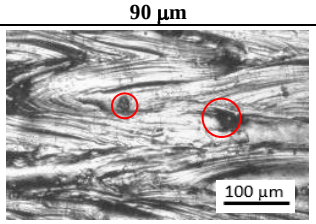	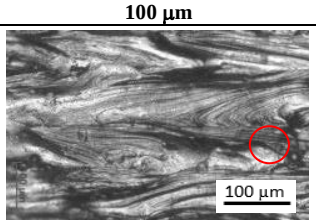
	Rescan		
Top view of single layers	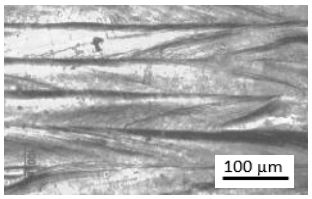	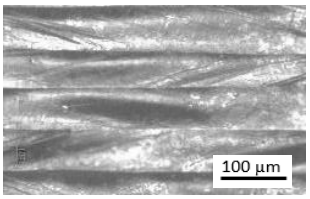	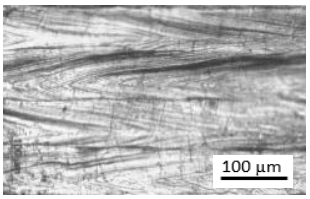

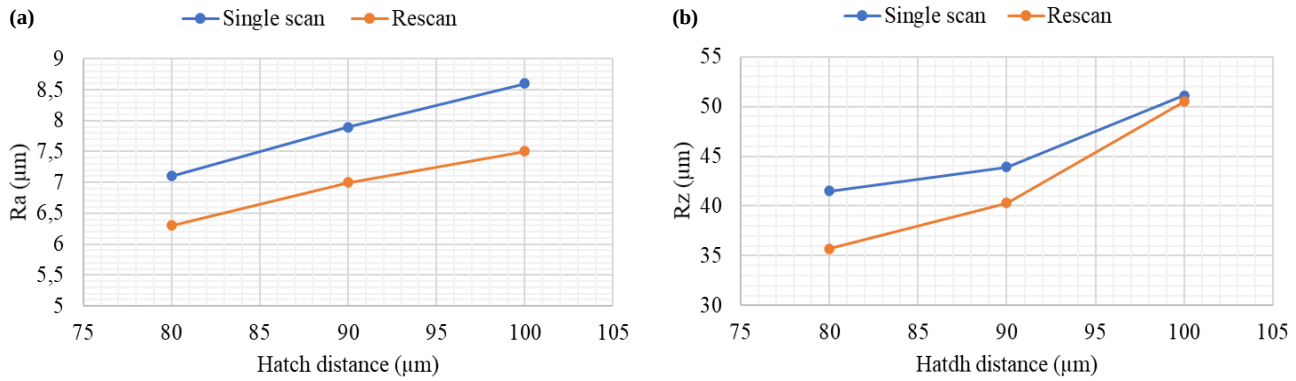

Figure 6. Surface roughness of in-situ alloyed Ti6Al4V-1 at% Cu at different hatch distances: (a) Ra and (b) Rz.

The presence of satellites on the surface of the single scan samples (Table 2 - single scan) increases the surface roughness of the samples (Figure 6). The single layers were rescanned (Table 2 - rescan), and the satellites were completely removed from the surface of the samples which have resulted in improving the surface roughness of the samples (Figure 6). It is well documented that the top surface roughness of LPBF parts is between 6 µm to 10 µm for *Ra* and >30 µm for *Rz* [17,35, 38,39]. *Rz* is the average distance between the highest peaks and the deepest valleys within the sampling length while the *Ra* is the arithmetic mean of all deviations of the sampling path length. The current experimental results fall within the expected values for both *Ra* and *Rz* (Figure 6). Rescanning lowers, the *Ra* and *Rz* value more than 30% (Figure 6).

As depicted by Figures 3(a-c), the tracks produced at a laser power of 170 W (the optimum laser power) are more regularly shaped as compared to tracks produced at laser powers of 150 W and 200 W. Therefore, it could be pointed out that within the optimum process parameter window the characteristics of the track are more regular, hence samples produce at the optimum process parameters would exabit relatively smooth surfaces.

Since rescanning would increase the cost of production due to the increase in machine time, for industrial applications only the final top layer of the LPBF built part should be rescanned.

From the EDS elemental mapping (Table 3) the distribution of the Cu in the Ti6Al4V alloy matrix was investigated. Generally, for all the hatch distances the distribution of the Cu in the Ti6Al4V was inhomogeneous after the single scan process (Table 3 - single scan). There were pockets of concentered Cu randomly distributed in the Ti6Al4V-1 at% Cu alloy matrix. The random distribution of the Cu could be due to the convective flow in the molten pool [21,40]. The temperature gradient in the molten pool due to the nature of the Gaussian laser beam induces recirculating flow (convective flow) within the molten pool which resulted in the dispersed and random distribution [32] of the concentrated pockets of Cu in the Ti6Al4V-1 at% Cu alloy matrix. The samples were rescanned, and the homogeneity was improved especially for samples at a hatch distance of 80 µm (Table 3 - rescan). The improvement in the homogeneity after the rescan is due to the increase in laser radiation absorption of the samples during the rescanning process. Bergström *et al.* [41] explained that the absorption of surfaces increases with roughness due to the onset of multiple scattering. The absorption of radiation increases significantly with roughness for metals which have a low absorptivity in the flat, smooth state, such as Cu. After the single scan of the Ti6Al4V and Cu powder mixture, the powder particles melted and created islands (satellites) of repeated solidification lines on the Ti6Al4V-1 at% Cu alloy matrix resulting in high surface roughness (Figure 6). The high

surface roughness after the single exposure of the powder bed increases the laser absorption during the rescanning which leads to higher temperatures and more prominent flow in the molten pool [42]. The prominent flow triggers a stirring effect in the molten pool that leads to the improvement in the homogeneity of the alloy after the rescanning process (Table 3). As explained by Yadroitsev *et al.* [24], the interaction of the laser beam with solid material can lead to higher energy input during the rescanning process due to the absence of new powder layer deposition. The higher energy input triggers the easy flowing of the molten metal with a large liquid surface which lead to the improvement in the homogeneity of the alloy.

The surface composition of the Cu in the Ti6Al4V alloy matrix was also investigated. It was noticed that Cu distribution at the surface of the alloy matrix was uneven after the single scan (Figure 7). The Cu composition at the surface of the alloy matrix becomes almost uniform after the rescanning process (Figure 7), due to the increasing temperature in the molten pool during the rescanning process. The prominent flow of the molten pool as a result of the higher energy input cause Cu to inter diffuse with the Ti6Al4V and formed homogenous alloy leading to the uniform distribution of the Cu at the surface of the Ti6Al4V-1 at% Cu alloy before the molten pool solidifies.

The cross-sections of the single layers were also analyzed (Table 4). The solidified molten layer forms a wavier-like shape as the result of the convective melt flow [21,24]. The penetration depth of the single layers after the rescanning strategy increase as compared to the penetration depth of the single scan samples (Table 4). The increase in the penetration depths after the rescanning process is due to the increase in the laser energy absorption as a result of the increase in the surface roughness after the first exposure [41]. The penetration depths of the layers produced at 100 µm hatch distance were quite deep, almost a 'V' shape due to less overlapping as compared to layers produced at 80 µm and 90 µm hatch distances. A careful observation revealed that layers produced at 80 µm hatch distance would yield optimum results.

Table 3. Elemental mapping of the Ti6Al4V-1 at% Cu top surface at different hatch distances.

	Single scan		
	80 µm	**90 µm**	**100 µm**
EDS Elemental mapping of top view	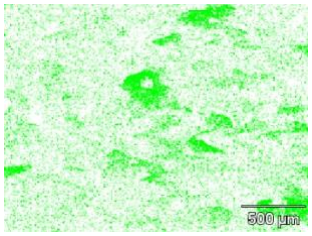	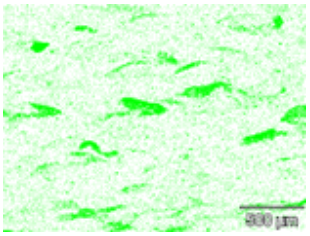	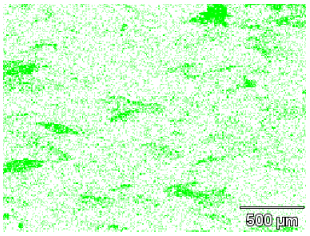
	Rescan		
EDS Elemental mapping of top view	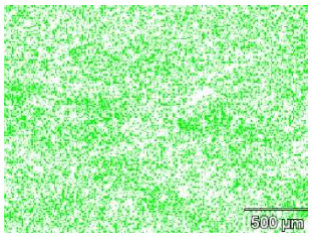	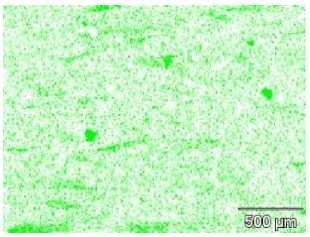	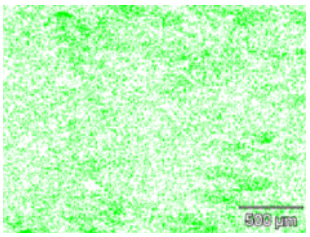

Table 4. Cross-section view of DMLS Ti6Al4V- 1 at% Cu at different hatch distances.

	Single scan		
	80 µm	**90 µm**	**100 µm**
Cross section			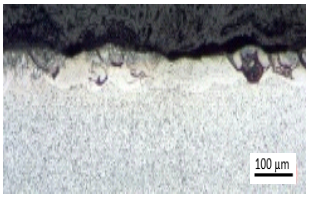
	Rescan		
Cross section			

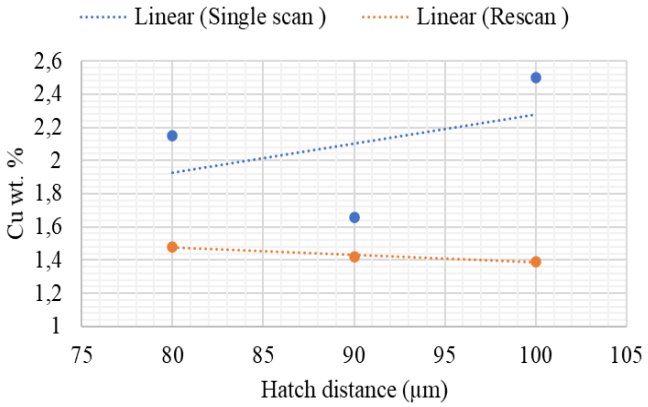

Figure 7. Average wt% of Cu near the DMLS surface of Ti6Al4V-1 at% Cu alloy at different hatch distances.

From the uniform homogenous distribution of the Cu in the Ti6Al4V- 1 at% Cu alloy matrix at hatch distance of 80 µm observed from the EDS elemental mapping (Table 3), the uniform surface concentration of Cu in the Ti6Al4V- 1 at% Cu alloy matrix (Figure 7), the low surface roughness value at 80 µm hatch distance (Figure 6) and the penetration depths after rescanning of the layers (Table 4): 80 µm hatch distance appears as the optimum hatch distance for manufacturing the Ti6Al4V- 1 at% Cu alloy. Hence the optimum process parameters arrived at after the experiment are: ***170 W, 1.0 ms^{-1} and hatch distance of 80 µm.***

4. Conclusions

The possibility of manufacturing biomedical implanted and surgical devices with antibacterial properties using LPBF technology has been demonstrated successfully. Optimum process parameters of 170 W, 1.0 ms^{-1} and hatch distance of 80 µm were arrived at after the investigation. The rescanning strategy was used to improve the homogeneity, surface concentration of Cu and surface roughness of the alloy. Successful *in situ* alloying Ti6Al4V- 1 at% Cu alloy would solve the problem of antibacterial agents falling off from the Ti6Al4V metal matrix. Gradually, the industry is approaching an era of mixing different elemental powders to produced novel alloys with tailored properties for specific biomedical and engineering applications using the LPBF manufacturing technology.

Acknowledgment

This work is based on the research supported by the South African Research Chairs Initiative of the Department of Science and Technology and National Research Foundation of South Africa (Grant No. 97994) and the Collaborative Program in Additive Manufacturing (Contract № CSIR-NLC-CPAM-18-MOA-CUT-01). The author would like to acknowledge the contribution of Prof. I. Yadroitsau, Prof. P. Krakhmalev and Dr. I. Yadroitsava who were his doctoral studies supervisors.

References

[1] V. R. Jablokov, M. J. Nutt, M. E. Richelsoph, and H. L. Freese, "The application of Ti-15Mo beta titanium alloy in high strength structural orthopaedic applications," *In Titanium, Niobium, Zirconium, and Tantalum for Medical and Surgical Applications, Journal of ASTM International*, vol. 2(8), 2006.

[2] M. Niinomi, "Mechanical biocompatibilities of titanium alloys for biomedical applications," *Journal of the Mechanical Behavior of Biomedical Materials*, vol. 1(1), pp. 30-42, 2008.

[3] W. M. Dunne, " Bacterial adhesion: seen any good biofilms lately?," *Clinical microbiology reviews*, vol. 15(2), pp. 155-166, 2002.

[4] L. Zhao, P. K. Chu, Y. Zhang, and Z. Wu, "Antibacterial coatings on titanium implants," *Journal of Biomedical Materials Research Part B: Applied Biomaterials*, vol. 19(1), pp. 470-480, 2009.

[5] T. C. Dzogbewu, and W. B. du Preez, "Additive manufacturing of titanium-based implants with metal-based antimicrobial agents," *Metals*, vol. 11(3), pp.453, 2021.

[6] C. Jung, L. Straumann, A. Kessler, U. Pieles, and M. de Wild, "Antibacterial copper deposited onto and into the oxide layer of titanium implants," *BioNanoMat*, vol. 15, pp. S180, 2014.

[7] L. Nan, W. C. Yang, Y. Q. Liu, H. Xu, Y. Li, M. Q. Lu, and K. Yang, "Antibacterial mechanism of copper-bearing antibacterial stainless steel against E. coli," *Journal of Materials Science and Technology*, vol. 24(2), pp. 197-201, 2008.

[8] T. Shirai, H. Tsuchiya, T. Shimizu, K. Ohtani, Y. Zen, and K. Tomita, "Prevention of pin tract infection with titanium-copper alloys," *Journal of Biomedical Materials Research Part B: Applied Biomaterials*, vol. 91(1), pp. 373-380, 2009.

[9] L. Ren, Z. Ma, M. Li, Y. Zhang, W. Liu, Z. Liao, and K. Yang, "Antibacterial properties of Ti–6Al–4V–xCu alloys," *Journal of Materials Science & Technology*, vol. 30(7), pp. 699-705, 2014.

[10] E. Zhang, "A new antibacterial titanium-copper sintered alloy: preparation and antibacterial property," *Materials Science & Engineering. C Materials for Biological Applications*, vol. 33(7), pp. 4280-4287, 2013.

[11] S. Das, "Physical aspects of process control in selective laser sintering of metals," *Advanced Engineering Materials*, vol. 5(10), pp. 701-711, 2003.

[12] T. C. Dzogbewu, "Laser powder bed fusion of Ti15Mo," *Results in Engineering*, vol. 7, pp. 100155, 2020.

[13] I. Yadroitsau, Selective laser melting: Direct manufacturing of 3D-objects by selective laser melting of metal powders, Lambert Academic Publishing, 2009.

[14] T. C. Dzogbewu, "Additive manufacturing of TiAl-based alloys," *Manufacturing Review*, vol. 7, pp. 35, 2020.

[15] A. Kinnear, T. C. Dzogbewu, I. Yadroitsev, P. Krakhmalev, and I. Yadroitsava, "Manufacturing, microstructure and mechanical properties of selective laser melted Ti6Al4V-Cu," in *in LiM" Lasers in manufacturing" conference*, Munich, 2017.

[16] T. C. Dzogbewu, and Y. D. Arthur, "Comparative studies of locally produced and imported low-carbon steels on the ghanaian market," *Journal of Natural Sciences*, vol. 1(1), pp. 15-22, 2013.

[17] EOS, "EOS titanium Ti64," EOS GmbH - Electro Optical Systems, 2014.

[18] T. C. Dzogbewu, "Laser powder bed fusion: evaluation of Ti15Mo single tracks," *Journal of Mechanical Engineering Research & Developments*, vol. 43(6), pp. 487-496, 2020.

[19] T. G. Spears, and S. A. Gold, "In-process sensing in selective laser melting (SLM) additive manufacturing," *Integrating Materials and Manufacturing Innovation*, vol. 5(1), pp. 1, 2016.

[20] T. C. Dzogbewu, I. Yadroitsev, P. Krakhmalev, I. Yadroitsava, and A. Du Plessis, "Optimal process parameters for in-situ alloyed Ti15Mo structures by Direct Metal Laser Sintering", *In SSF 2017-The 28th Annual International Solid Freeform Fabrication Symposium*, Austin, August 7-9, 2017 (pp. 75-96). University of Texas, 2017.

[21] C. L. Chan, J. Mazumder, and M. M. Chen, "Three-dimensional axisymmetric model for convection in laser-melted pools," *Materials Science and Technology*, vol. 39(4), pp. 306-311, 1987.

[22] S. A. Khairallah, A. T. Anderson, A. Rubenchik, and W. E. King, "Laser powder-bed fusion additive manufacturing: Physics of complex melt flow and formation mechanisms of pores, spatter, and denudation zones," *Acta Materialia*, vol. 108, pp. 36-45, 2016.

[23] L. Rayleigh, "On the instability of a cylinder of viscous liquid under capillary force," *The London, Edinburgh, and Dublin Philosophical Magazine and Journal of Science*, vol. 34(207), pp. 145-154, 1892.

[24] I. Yadroitsev, A. Gusarov, I. Yadroitsava, and I. Smurov, "Single track formation in selective laser melting of metal powders," *Journal of Materials Processing Technology*, vol. 210(12), pp. 1624-1631, 2010.

[25] C. Körner, E. Attar, and P. Heinl, "Mesoscopic simulation of selective beam melting processes," *Journal of Materials Processing Technology*, vol. 211(6), pp. 978-987, 2011.

[26] I. Yadroitsev, P. Krakhmalev, I. Yadroitsava, S. Johansson, and I. Smurov, "Energy input effect on morphology and microstructure of selective laser melting single track from metallic powder," *Journal of Materials Processing Technology*, vol. 213(4), pp. 606-613, 2013.

[27] W. E. King, H. D. Barth, V. M. Castillo, G. F. Gallegos, J. W. Gibbs, D. E. Hahn, C. Kamath, and A. M. Rubenchik, "Observation of keyhole-mode laser melting in laser powder-bed fusion additive manufacturing," *Journal of Materials Processing Technology*, vol. 214(12), pp. 2915-2925, 2014.

[28] T. W. Eagar, and N. S. Tsai, "Temperature fields produced by traveling distributed heat sources," *Welding Journal*, vol. 62(12), pp. 346-355, 1983.

[29] J. Yang, J. Han, H. Yu, J. Yin, M. Gao, Z. Wang, and X. Zeng, "Role of molten pool mode on formability, microstructure and mechanical properties of selective laser melted Ti-6Al-4V alloy," *Materials & Design*, vol. 110, pp. 558-570, 2016.

[30] D. B. Hann, J. Lammi, and J. Folkes, "A simple methodology for predicting laser-weld properties from material and laser parameters," *Journal of Physics D: Applied Physics*, vol. 44(44), pp. 445401, 2011.

[31] A. Klassen, and K. Carolin, "Modelling of electron beam absorption in complex geometries," *Journal of Physics D: Applied Physics*, vol. 47(6), pp. 065307, 2014.

[32] A. Zenani, T. C. Dzogbewu, W. B. du Preez, and I. Yadroitsev, "Optimum process parameters for direct metal laser sintering of Ti6Al powder blend," *Universal journal of mechanial engineering*, vol. 8(4), pp. 170-182, 2020.

[33] C. Körner, A. Bauereiß, and E. Attar, "Fundamental consolidation mechanisms during selective beam melting of powder," *Modelling and Simulation in Materials Science and Engineering*, vol. 21(8), p. 085011, 2013.

[34] S. A. Khairallah, and A. Anderson, "Mesoscopic simulation model of selective laser melting of stainless steel powder," *Journal of Materials Processing Technology*, vol. 214(11), pp. 2627-2636, 2014.

[35] C. Qiu, C. Panwisawas, M. Ward, H. C. Basoalto, J. W. Brooks, and M. M. Attallah, "On the role of melt flow into the surface structure and porosity development during selective laser melting," *Acta Materialia*, vol. 96, pp. 72-79, 2015.

[36] G. A. Longhitano, M. A. Larosa, A. L. J. Munhoz, C. A. D. C. Zavaglia, and M. C. F. Ierardi, "Surface finishes for Ti-6Al-4V alloy produced by direct metal laser sintering," *Materials Research*, vol. 18(4), pp. 838-842, 2015.

[37] X. Liu, P. K. Chu, and C. Ding, "Surface modification of titanium, titanium alloys, and related materials for biomedical applications," *Materials Science and Engineering: R: Reports*, vol. 47(3), pp. 49-121, 2004.

[38] T. C. Dzogbewu, "Laser powder bed fusion of Ti6Al4V lattice structures and their applications," *Journal of Metals, Materials and Minerals*, vol. 30(4), 2020.

[39] J. Maisonneuve, C. Colin, and P. Aubry, "Profile Project: direct manufacturing of aerospace components by laser cladding and laser sintering," Scottsdale, USA, 2007.

[40] B. Duleba, F. Greškovič, and J. W. Sikora, "Materials and finishing methods of DMLS manufactured parts," *Transfer Inovácií*, vol. 21, pp. 143-148, 2011.

[41] D. Bergström, J. Powell, and A. F. H. Kaplan, "A ray-tracing analysis of the absorption of light by smooth and rough metal surfaces," *Journal of Applied Physics*, vol. 101(11), pp. 113504-113504, 2007.

[42] M. P. P. Gharbi, C. Gorny, M. Carin, S. Morville, P. Le Masson, D. Carron, and R. Fabbro, "Influence of various process conditions on surface finishes induced by the direct metal deposition laser technique on a Ti–6Al–4V alloy," *Journal of materials processing technology*, vol. 213(5), pp. 791-800, 2013.